Analysis of a calibration method for non-stationary CVD multi-layered graphene-based gas sensors

Ricciardella, Filiberto; Polichetti, Tiziana; Vollebregt, Sten; Alfano, Brigida; Massera, Ettore; Sarro, Pasqualina M.

DOI
10.1088/1361-6528/ab2aac

Publication date
2019

Document Version
Final published version

Published in
Nanotechnology

Citation (APA)
Ricciardella, F., Polichetti, T., Vollebregt, S., Alfano, B., Massera, E., & Sarro, P. M. (2019). Analysis of a calibration method for non-stationary CVD multi-layered graphene-based gas sensors. *Nanotechnology*, *30*(38), 1-8. Article 385501. https://doi.org/10.1088/1361-6528/ab2aac

PAPER

Analysis of a calibration method for non-stationary CVD multi-layered graphene-based gas sensors

IOP Publishing Nanotechnology
Nanotechnology 30 (2019) 385501 (8pp) https://doi.org/10.1088/1361-6528/ab2aac

Analysis of a calibration method for non-stationary CVD multi-layered graphene-based gas sensors

Filiberto Ricciardella[1], Tiziana Polichetti[2], Sten Vollebregt[1], Brigida Alfano[2], Ettore Massera[2] and Pasqualina M Sarro[1]

[1] Department of Microelectronics, Delft University of Technology, Feldmannweg 17, 2628 CT Delft, The Netherlands
[2] ENEA Research Center, Piazzale Enrico Fermi, 1, I-80055 Portici (Napoli), Italy

E-mail: filiberto.ricciardella@gmail.com

Received 23 April 2019, revised 23 May 2019
Accepted for publication 18 June 2019
Published 11 July 2019

Abstract

Limitations such as lack of detected stationary signal and slow signal recovery after detection currently affect graphene-based chemi-sensors operating at room temperature. In this work, we model the behavior of a sensor in a test chamber having limited volume and simulating the environmental conditions. From this model, we mathematically derive the calibration method for the sensor. The approach, focused on the time differential of the signal output, is tested on multi-layered graphene (MLG)-based sensors towards the chosen target gas (nitrogen dioxide) in the range from 0.12 to 1.32 ppm. MLG acting as sensing layer is synthesized by chemical vapor deposition. Our study paves the route for a wider applicability of the analysis to calibrate the class of devices affected by non-stationary and recovery issues.

Supplementary material for this article is available online

Keywords: graphene, gas sensors, signal steady state and recovery, time-differential signal output, calibration, NO_2

(Some figures may appear in colour only in the online journal)

1. Introduction

The absence of detected steady-state signal and the slow and incomplete signal recovery represent two longstanding hindrances which still affect solid state gas sensors working at room temperature (RT) [1, 2]. Graphene-based gas sensors are not immune from these drawbacks [3, 4]. Since 2007, when such kind of sensor was originally fabricated [5], a great deal of theoretical and experimental works on graphene-based gas sensors has been presented in literature [6]. However, up to now only a few studies have reported the mentioned inherent bottlenecks [3, 4, 7–9] even though these limits can hamper the actual device application. For instance, Schedin *et al* already mentioned the lack of steady-state signals in their first work on graphene-based gas sensor, claiming that even 'during long exposures to small concentrations (parts per millions) of active gases, the devices did not saturate the detected signal indicating a cumulative effect of chemical doping in graphene' [5]. A partial stable signal can be observed in that paper, when the sensors are exposed to a limited volume of the chemicals rather than a constant flow [5]. Devices showing a complete stationary behavior were reported by Melios and co-workers after exposing the sensors for 2 h [10]. Sensors not achieving a steady-state were observed by several authors [3, 4, 11–13]. We also reported the same behavior in previous works dealing with graphene-sensors based on material prepared by chemical vapor deposition (CVD) and other techniques [14–18]. A possible explanation may be sought in the huge amount of adsorption sites[18] that are not completely saturated during the exposure to the gas. Even though the findings demonstrate that the feature is common to graphene synthesized by different techniques and other bi-dimensional materials [19, 20], plenty of investigation is still required to further address this issue.

The mechanisms mostly involved in the interaction between graphene and the gas molecules are chemi-sorption and physi-sorption. The former is attributed to the formation of strong chemical bonds, involving adsorption energy in the range of eV. As such, the chemi-sorption involves higher energies than the physi-sorption, characterized by weaker physical interactions between analytes and sensing material, such as van der Waals forces. The effect of the two processes reflects differently on the desorption time, it being longer or shorter for chemi- or physi-sorption, respectively [21, 22]. Especially when the species are chemisorbed, poisoning of the sensors can be experienced as well as a worsening of the performances [4, 19], dramatically compromising the further utilization of the sensors. To facilitate the desorption and allow the formation of a free interface on the sensitive layer, the most widely adopted methods aim at increasing the analyte molecule mobility by an external supply of energy, such as ultraviolet light (UV) irradiation [5, 23–26], thermal treatment [5, 10, 20, 27, 28] or exposure to an electric field [29]. For instance, Chen and his team [24] were able to detect concentrations down to parts per trillion, under inert atmosphere, although by continuously illuminating with UV radiations to clean *in situ* the sensing material. Similarly, Schedin *et al* found that UV under vacuum or annealing at 150 °C can restore the state of the devices after analyte exposure [5]. The annealing procedure was proved to work successfully also for carbon nanotube-based sensors: the devices were kept at 150 °C to speed up gas desorption, while the test chamber was flushed with pure dry air for 1 h after each series of successive gas injections. When the airflow was interrupted, the sensors were left at ambient temperature for 12 h such that a full restoration of the baseline resistance was reached. In this case, operating at RT, the NO_2 minimum detectable concentration of 500 ppb (parts per billion) was achieved [11]. Leghrib and Llobet as well as Melios *et al* demonstrated that the cleaning after the gas exposure was promoted by raising the temperature of the carbon nanotube- and graphene-based sensors above 100 °C, while the carrier gas was injected in the chamber [10, 30]. All the aforementioned techniques aim at making the sensors reusable, although require a significant complexity in the experimental setup. On one side they reveal particularly advantageous for fundamental investigations, even allowing to achieve exceptional performances and detect extremely low gas concentrations. On the other side, the solutions are not easy to implement for practical applications and especially not useful when working at RT. The limitations hereby discussed strongly impact two relevant parameters of the sensors, such as the response time and the percentage variation of the current induced by the analyte exposure. The response time is in fact the time required for reaching 90% of the steady-state signal magnitude [31, 32].

Also the calibration of the sensors becomes hardly manageable, unless the sensors are undergone to very long exposures steps. This solution, however, appears unfeasible when the gas concentrations change frequently, as usually happens in the environmental conditions. In our previous work, we have introduced a post-process technique based on the time differential of the signal output (TDSO) which allowed at once to counteract both the lack of steady-state signals and the poor recovery [15]. In that paper, we applied the method to calibrate gas sensors based on multi-layered graphene (MLG) derived from inks. In another work, we have shown that TDSO approach works properly even for sensors based on MLG grown by CVD [33].

In this paper, starting from the final outcomes reported in [31], we focus on the analytical derivation of the method based on the TDSO. We present both experimental results and numerical simulations to validate the model. The experiments were carried out on a device based on MLG grown by CVD. We performed the sensing analysis at RT and relative humidity (RH) set at 50%, using nitrogen dioxide (NO_2) as target gas. We chose NO_2 because of the stronger sensitivity of MLG towards that analyte compared to other species, as reported in our previous works [14, 16]. Finally, we prove the validity of the model showing the dependence between the gas concentration and TDSO, which allows the calibration of the sensors presenting no-steady-state and poor recovery.

2. Experimental sections

2.1. Material and device preparation

The MLG film was grown by CVD at ∼1000 °C on pre-patterned Mo catalyst in an AIXTRON BlackMagic Pro, via a mixture of $Ar/H_2/CH_4$ at a pressure of 25 mbar.

The sensor was based on CVD-grown MLG and directly fabricated on the pre-patterned structures [17]. The graphene is contacted by Cr/Au electrodes which were deposited using e-beam evaporation in combination with a lift-off in NMP. The device has a sensing area of 1030 μm^2 (figure 1).

I–V measurements were performed on the prepared MLG-based resistor in the −0.5, 0.5 V range, through a semi-automatic probe-station equipped with an Agilent 4156C semiconductor parameter analyzer. The device was then bonded by using Al wires (30 μm diameter) to perform the sensing measurements.

2.2. Gas sensing tests

Gas detection experiments were carried out in a customized gas sensor characterization system (GSCS) able to mimic the environmental conditions in terms of temperature, pressure and RH. These parameters were set at (22 ± 2) °C, (1.00 ± 0.05) bar and 50%, respectively. The measurements were performed selecting NO_2 as target gas under a flow of N_2 as buffer gas through the sensor chamber (figure 2). The total flow was kept at 500 sccm.

The GSCS consists of a stainless steel chamber (40 cl), placed in a thermostatic box and provided with an electrical grounded connector for bias and conductance measurements. Different gases concentrations were obtained by programmable mass flow controllers (MFCs). During the measurements, the sensors were biased at a constant DC voltage equal to 1 V with a Precision Power Supply (TTi QL355T) and the

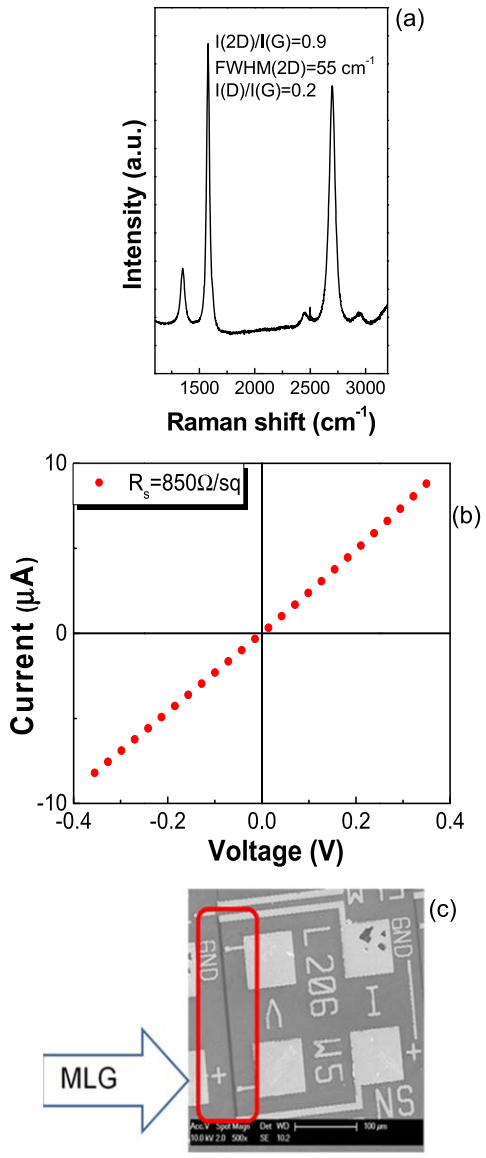

Figure 1. (a) Representative Raman spectrum of MLG averaged on 100 points (see figure S1 is available online at stacks.iop.org/NANO/30/385501/mmedia). The spectrum is normalized to the G band. The values of both FWHM(2D) and $I(2D)/I(G)$ show that the sensing layer is definitely composed by MLG. The ratio $I(D)/I(G)$ indicates the level of defectiveness. (b) *I–V* characteristic and (c) SEM image of the device. The bar covered with MLG is 206 μm long and 5 μm large (red rectangle).

current values were recorded by a high resolution picoammeter (Keithley 6485).

2.3. Test protocols

The first protocol to which the sensors were subjected, in the following addressed as *Test* 1, consisted of a single exposure at 1 ppm of analyte flowed through the chamber for 10 min. The baseline and recovery phases, respectively preceding and following the exposure window, consisted of 20 min long exposures to the buffer gas.

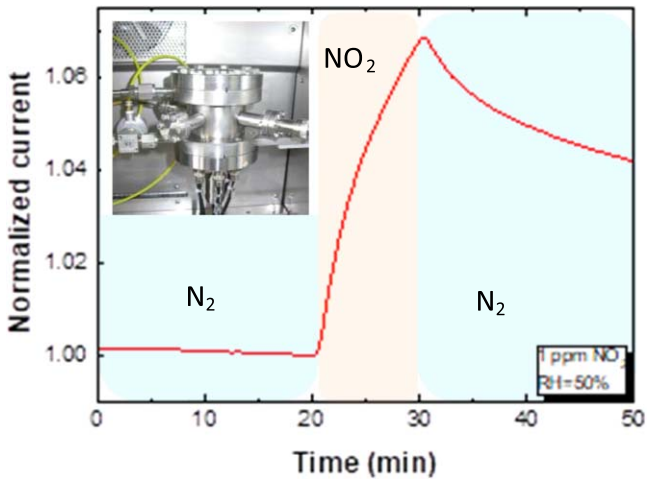

Figure 2. Normalized current of the chemi-resistor upon exposure to *Test* 1. Inset: image of the experimental setup where the sensing tests were performed.

Test 2 was composed of five sequential pulses of the analyte at 1 ppm. The protocol is equivalent to five subsequent repetitions of *Test* 1.

During *Test* 3 the devices were subjected to 11 sequential pulses at different concentrations of analyte ranging from 1.32 down to 0.12 ppm (see table 1). Each step lasted 4 min, preceded and followed by 20 min long baseline and recovery phases, respectively.

Finally, *Test* 4 was similar to *Test* 3 in terms of injected gas concentrations, the only difference concerned the sequential pulses in the protocol, which were set as reported in table 1.

3. Results and discussion

Raman spectroscopy (figure 1(a)) show that the material grown by CVD is composed of MLG, as established by the ratio $I(2D)/I(G)$ and the full width at half maximum of 2D [16–18]. Atomic force microscopy and scanning electron microscopy confirmed the layered structure of the sensing material (see figure S1).

Figure 1(b) shows the *I–V* characteristic measured on the device reported in figure 1(c).

The linearity of the *I–V* curves testifies that the MLG-based strips are in Ohmic contact with the Cr/Au pads.

Figure 2 shows the current behavior of the sensor during *Test* 1, consisting of a single pulse of 1 ppm of NO_2 (more details in experimental section). The signal is normalized to the value I_{in}, which is the current immediately prior to the gas exposure. When the device, acting as a chemi-resistor, was exposed to the gas, a charge transfer reaction occurred between the sensing materials and the adsorbed gas [20]. The change of the material resistance induced the rise of the current due to the p-type doping of MLG and the acceptor-like nature of NO_2 [5, 15].

The absence of a steady-state signal along with the slow recovery after the exposure step is clearly noticed in the graph (figure 2) [15]. This behavior is further highlighted in

Table 1. Description of protocols called *Test* 3 and *Test* 4 performed on the gas sensors.

	NO_2 concentration (ppm)										
	I	II	III	IV	V	VI	VII	VIII	IX	X	XI
Test 3	1.32	1.20	1.08	0.96	0.84	0.72	0.60	0.48	0.36	0.24	0.12
Test 4	1.32	0.84	1.20	0.72	1.08	0.60	0.48	0.36	0.96	0.24	0.12

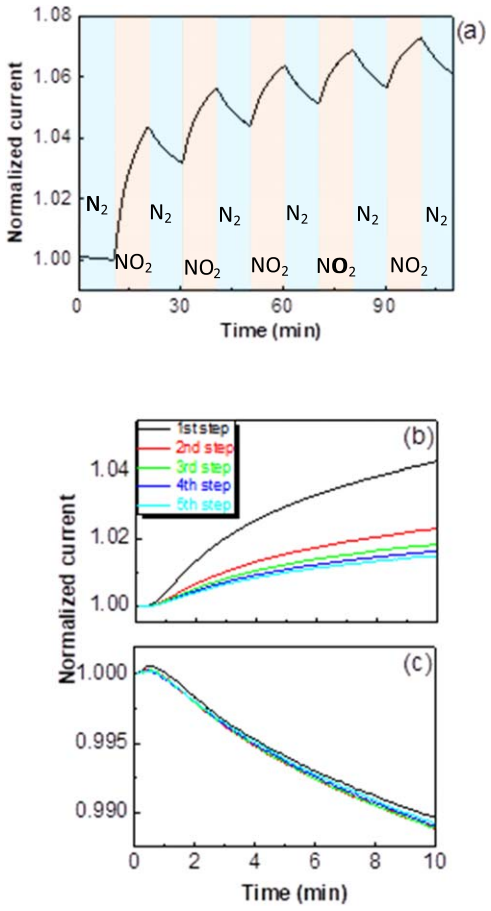

Figure 3. (a) Real-time current behaviors of graphene-based chemiresistor upon exposure to five sequential NO_2 pulses (pale orange rectangles) at concentration of 1 ppm in N_2 atmosphere. The exposure and recovery windows (pale blue rectangles) lasted 10 min (b) rising and (c) decreasing part of the signal recorded during the sequential exposure and recovery windows reported in panel (a). The rising and decreasing signals are normalized to the current at the gas inlet and outlet of each exposure, respectively.

figure 3(a), where the real-time current behavior during *Test* 2 is reported. The signal is normalized to I_{in}, i.e. the current at the gas inlet of the first exposure. For the sake of clarity, the signals recorded both during the sequential exposures and the recovery phases were grouped in figures 3(b) and (c), respectively.

Looking at the current variations (figures 3(a), (b)), the decrease of the responsiveness can be observed for each subsequent step, where the responsiveness is defined as $\Delta I/I_0 = (I_{\max} - I_0)/I_0$. I_0 indicates the current in the initial, unperturbed state of each exposure and I_{max} the maximum of the current value when the analyte flow is stopped. Because of the absence of the steady-state, the term responsiveness was used instead of response [34]. The two parameters differ only for I_f used in the response definition instead of I_{max}, where I_f is the value of the current reached at the steady-state.

Table 2. Responsiveness and recovery time values determined from figure 3.

Step number	Responsiveness (%)	Recovery time (s)
I	4.3	640 ± 30
II	2.3	640 ± 20
III	1.8	710 ± 30
IV	1.6	710 ± 30
V	1.5	740 ± 30

Similarly to the results in figure 3(a), the degradation of the signal was observed by Ko *et al* [35] although in that paper graphene is prepared by mechanical exfoliation and not by CVD as in our case. This feature further attests that the lack of steady-state and the poisoning effect do not depend on the particular technique of material production. Those phenomena are more related to the material itself, as proved by both theoretical and experimental works [4, 6, 15, 19, 36, 37]. From the sensing point of view, the major differences related to different techniques of synthesis is the energy characterizing the adsorption sites [6, 18]. Noteworthy, we chose the behavior of the sensors as a mean of comparison since in this paper we mostly focus on the analysis of a method. Comparing the performances of the device with those reported in the literature can mislead the readers, being the analysis of the performances out of the focus of the paper.

The responsiveness values for each exposure step (figure 3(a)) and the recovery time are reported in table 2. The latter parameter was determined by the exponential fit of the curves during the N_2 purging (see figure S2), while the recovery time is the time required to reach the 10% of the signal magnitude [38–40].

The differences in terms of the sensor responsiveness between the first and the other four steps of the complete cycle (figure 3(a)) are a straightforward indication that the poisoning can affect the device performance.

After the first exposure, the responsiveness value becomes progressively lower due to the adsorbed molecules which are not completely removed from the MLG once NO_2 is switched off [41].

In other words, the more strictly adsorbed molecules remain attached to MLG whilst the molecules cleaned away by the buffer gas (N_2) are those weakly bonded to the sensing layer. This evidence is corroborated by the substantial uniformity of the recovery time (figure 3(c) and table 2).

The poisoning effect due to the trapped gas molecules determines, in turn, the upshift of I_0, which is the

initial, unperturbed state between two subsequent pulses (figure 3(a)).

What is practically experienced is a sort of ripple effect. Since the desorption is quite poor at RT, especially without supplying any additional energy, the devices are not able to completely get rid of the adsorbed molecules. The gas trapped is progressively increased after each step. Consequently, a decreasing current variation can be measured in the subsequent sensing steps. Less intense responsiveness is then induced, because of the higher number of occupied adsorbing sites.

The analysis presented so far describes the sensor behaving as a device able to continuously integrate gas molecules, hardly releasing them, especially if no external energy is supplied. This integrating behavior of the sensor was presented elsewhere, although MLG was synthetized by liquid phase exfoliation (LPE) instead of CVD [15]. Based on our previous results [15] and starting from the quantitative model recently developed by Mackin and co-workers [42], hereby we assume that the observed current during the adsorption window can be described by the following equation:

$$I(t) = AC^{\alpha}(1 - e^{-\frac{t-t_0}{\tau_1}}). \quad (1)$$

The formula is composed by two terms, besides the amplification factor A determined by the electronics of the setup. C^{α} is the gas concentration injected in the test chamber where α is a parameter correlated to the sensing mechanism of the sensor. That parameter is independent of time, material and environmental conditions and ranges between 0.5 for metal oxide (MO_x) and 1 for electrochemical sensors (EC) [43]. In our case, it is reasonable to assume the same range for α.

MO_x and graphene-based chemi-resistors in fact have almost the same transduction mechanism. The main difference between the two classes of sensors is that for MO_x the adsorption is driven by the ions while in the second case the transduction is due to the charge transfer [20]. The term in the parenthesis (equation (1)) describes the behavior of the sensor, being t_0 the instant when the analyte is injected in the test chamber and τ_1 is the typical rise time of the sensor. If we assume the gas concentration constant in equation (1), as a first approximation, the formula describes the time dependency of a transient phenomenon between two stationary states, such as for the capacitor charge. Analytically, the stationary signal is reached for $t \rightarrow \infty$. This analytical condition means essentially a quite long exposure time [10]. Such a sensor, however, is not practical, especially for applications where the gas concentrations may change rapidly, e.g. in the outdoor scenario. As determined by the theory of the capacitor charge, in a time equal to $3\tau_1$ it is expected that 95% of the steady-state signal is reached. From the fitting of the adsorbing phase, $3\tau_1$ is estimated to be around 20 min in our case. For practical applications, it could be attractive to predict the steady-state response of the sensor in the exposure range of a few minutes. In such a short range of exposure, the sensor hereby presented is not stabilized, but still in the ramp up phase of the signal.

As a matter of fact, the gas concentration in a test chamber with a fixed volume is neither constant nor follows the Heaviside function of time. The kinetics of the gas does not follow directly the opening of the valve. In fact, the schematics reported so far (e.g. blue rectangles in figure 3(a)) simply depict the gas pulses. As a consequence of the time-dependence of the gas in chamber, equation (1) should be corrected to:

$$I(t) = AC^{\alpha}(1 - e^{-\frac{t-t_0}{\tau_1}})(1 - e^{-\frac{t-t_0}{\tau_2}})^{\alpha}, \quad (2)$$

where the second parenthesis expresses the time-dependency of $C^{\alpha}(t)$ and τ_2 is the time to fill-in the test chamber. The second parenthesis describes again the transient between two stationary states in the chamber. The initial state is determined by the presence of only buffer gas whilst the final state is reached when the gas concentration completely fills up the chamber. The injection of NO_2 in the test chamber is driven by the MFCs. The MFCs provide a force to keep constant the flow such that the injection cannot be assumed as a diffusion process. The MFCs play again a role similar to that of the electric field during the charging of a capacitor.

Non-stationary behavior and scarce analyte desorption of the sensors were investigated and turned into advantages by introducing TDSO [15]. The method consisted in differentiating the output of the sensor. Then, the maxima of the differential output were plotted as function of the gas concentration to calibrate the sensor. In the present work, the choice of TDSO is physically and analytically proved on a sensor based on MLG grown by CVD. The introduction of TDSO is driven by the concept that the derivative of the Heaviside function is the δ-Dirac. In fact, if the gas concentration was constant such as in equation (1) (e.g. assuming the concentration as governed by the Heaviside function as first approximation), the differential would have been peaked at $t = t_0$, exactly when the gas would have entered the chamber (equation (3)). Also the intensity of the TDSO peak would be proportional to the gas concentration according to the following equation:

$$\left(\frac{\partial I}{\partial t}\right)_{t=t_0} = \frac{AC^{\alpha}}{\tau_1}. \quad (3)$$

The blue curve in figure 4(a) reports the TDSO of equation (1), resulting from the numerical simulation of *Test* 1. For the sake of simplicity, $\alpha = 1$. As parameters in the mathematical model, we adopted τ_1 and τ_2 equal to 300 and 50 s, respectively. The value of τ_1 is determined by the fit of the graphs during the exposure window (figure 2). The value of τ_2 is estimated on the basis of test chamber volume and the gas flow (see experimental section). The red curve (figure 4(a)) shows the TDSO of equation (2).

If the concentration is a function of time (equation (2) versus equation (1)), the signals are slightly different. In both cases the peak is present but it is shifted to $t = t_1$ instead of lying at $t = t_0$ (figure 4(b)). The same result is experimentally verified (figures 4(c), (d)). Figure 4(b) also shows that the intensity of the

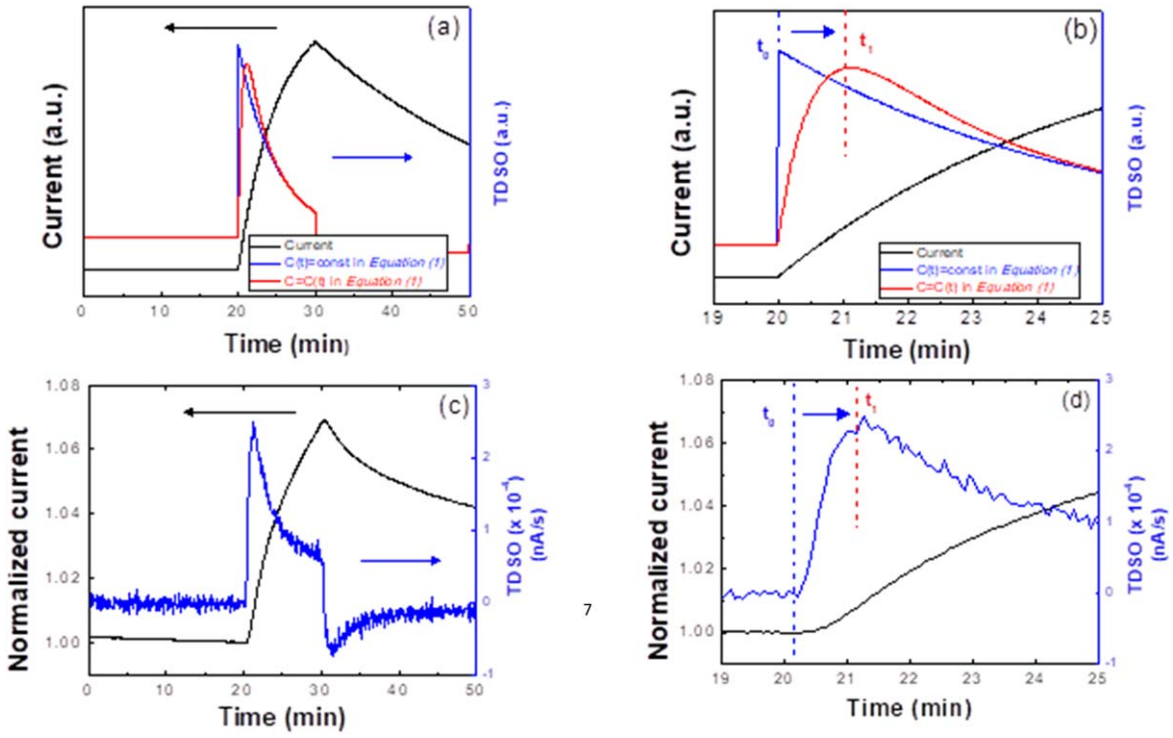

Figure 4. (a) Current (black curve) obtained by numerical simulation of *Test* 1. The differential current is showed applying TDSO (blue curve) and assuming the gas concentration constant or time-dependent (red curve), as reported in equation (2). (b) Close-up of the peak position of the panel (a) highlighting the time shift indicated by the blue arrow. (c) Normalized current (black curve) of the *Device* 2*B* upon exposure to *Test* 1 and TDSO (blue curve). (d) Close-up of the peak position of the panel (c) highlighting the time shift indicated by the blue arrow.

red curve is lower compared to that of the blue one. To analytically demonstrate this result, we should need to determine the maximum of TDSO[15] applied twice on equation (2).

Since the goal of the presented discussion is to determine the contributions of τ_1 and τ_2 to the maximum of TDSO, we adopted the following solution which avoids further mathematical complexity (see equation S1). Firstly, we expanded in power series TDSO[15], stopping it at the first order. Then, we applied again TDSO [15] on the obtained result (equation (4)):

$$\frac{\partial^2 I}{\partial t^2} = \frac{2AC}{\tau_1\tau_2}\left[1 - \frac{\tau_1+\tau_2}{\tau_1\tau_2}(t-t_0)\right]. \quad (4)$$

Making the term in brackets zero, we found out that the maximum is thus located at $t_{max} = t_0 + \tau_1\tau_2/(\tau_1+\tau_2)$ and the intensity of TDSO is estimated to be:

$$\left(\frac{\partial I}{\partial t}\right)_{t=t_{max}} = \frac{AC}{\tau_1+\tau_2}. \quad (5)$$

Even though equation (5) represents an approximated result, it clearly shows the effect of the time to fill-in the test chamber (τ_2) compared to equation (3). Introducing the term that describes the gas behavior in the chamber definitely affects the TDSO in both shifting ($t_{max} = t_0 + \tau_1\tau_2/(\tau_1+\tau_2)$) and lowering the maximum of the peak. The limit $\tau_2 \to 0$ further proves the validity of our hypothesis. In case $\tau_2 \to 0$, it results that $t_{max} \to t_0$, equation (5) would tend to equation (3) and TDSO would tend to the δ-Dirac (blue curve in figure 4(a)) (figure S3).

Equation (5) also confirms that the intensity of TDSO maxima are uniquely correlated to the gas concentration as empirically proved in our previous works [15, 33]. Further investigation is ongoing to carefully address and compensate the effect of the test chamber filling.

To prove the conclusions reached through the numerical simulations, we performed a test (*Test* 3 in experimental section), in which each gas concentration is injected for 4 min. This exposure setting ensures that the sensor is still in the ramp up phase of the adsorption process. Our goal is, in fact, to exploit the hampering non-stationary behavior of the sensors into a key point for the device calibration. Figure 5 shows the results after processing the signal with TDSO protocol.

The maxima of TDSO are the most meaningful values to analyze based on equation (3). These maxima plotted as a function of NO_2 concentration show a robust correlation (figure 6). In particular, the linear fit of the scatter plot is characterized by the value of R^2 equal to 0.98 (red line in figure 6).

The linear dependency by the NO_2 concentration points out that the filling of the test chamber only affects the time shift and the attenuation of the peak, regardless the injected gas concentration. The fit even reveals that the assumption $\alpha = 1$ provides the best correlation with NO_2 concentration (see figure S4).

To absolutely ensure that TDSO and the calibration method are not dependent on the specific executed protocol,

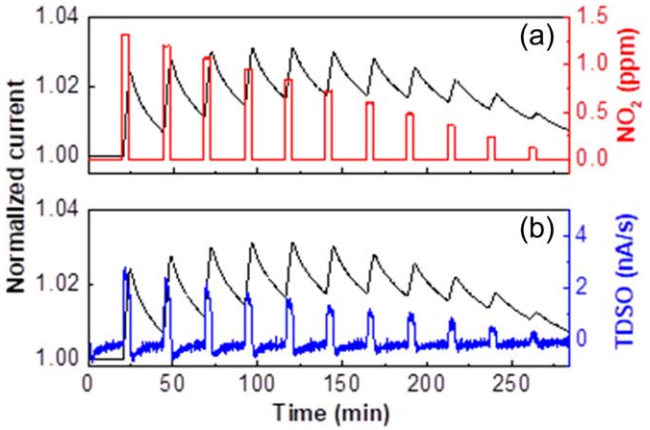

Figure 5. (a) Real-time current behavior (black curve) of Device 2B during *Test* 3 (red rectangles) setting RH level at 50%. (b) Differential current (blue curve) overlapped to the current signal (black curve) reported in panel (a). In both panels, the current is normalized to the value of the initial unperturbed state of the first exposure.

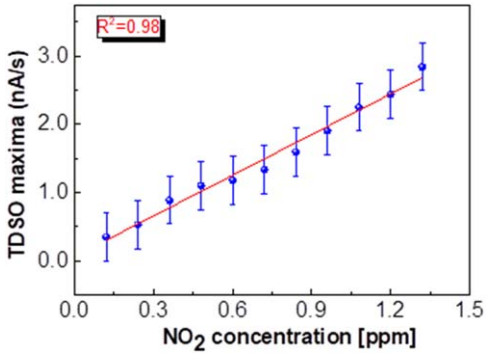

Figure 6. Maxima of the differential curve from figure 5 as function of the NO_2 concentration.

we performed *Test* 4 (see experimental section). That test simulates the same number of gas concentrations pulses as *Test* 3, but in a random way (figure 7).

The outcomes in figure 7 are comparable with those in figure 6, especially as far as the linear trend of the maxima as function of NO_2 concentration is concerned (figure 7(c)).

If we define the slope of the calibration plot as differential sensitivity, the comparison between the different tests appears more straightforward. We estimated values of differential sensitivity equal to (1.98 ± 0.08) and (2.01 ± 0.16) $nA/(s\,ppm)$ for *Test* 3 and *Test* 4, respectively.

The findings determined through TDSO firstly confirm that the model based on equation (2) properly describes the behavior of the sensor in the test chamber. Then, we have demonstrated that the calibration approach is independent by both the adopted protocol and the technique to synthesize the sensing material, since MLG-based on CVD (used in this paper) or LPE [15] have provided substantial analogies. In our previous work, we have empirically applied TDSO protocol to sensors of different size [33]. Those results showed that the method is even independent by the sensing area.

The breakthrough will be the application of this method on no-stationary sensors working in outdoor conditions,

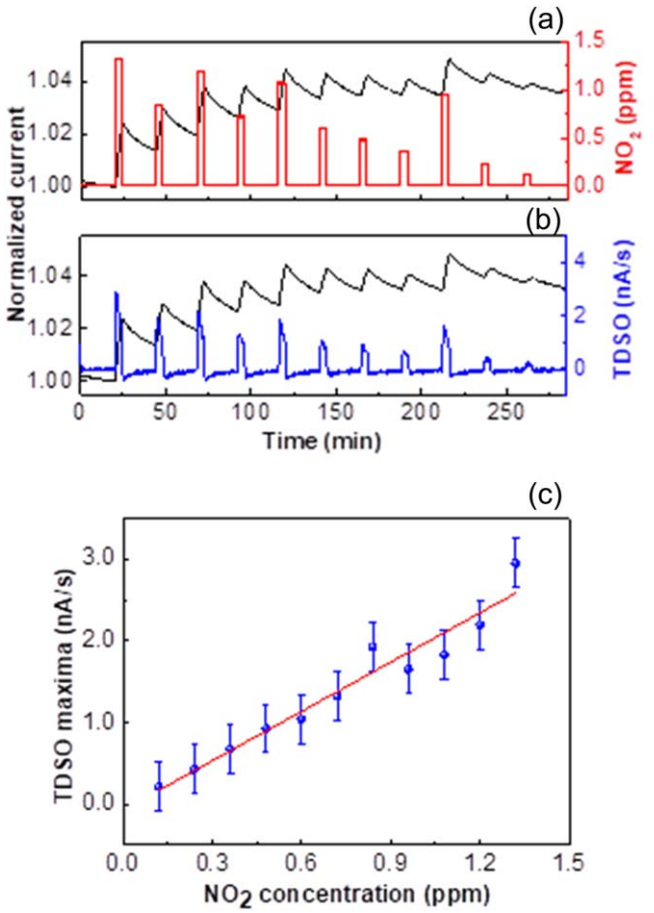

Figure 7. (a) Real-time current behavior of *Device* 2*B* towards *Test* 4 (red rectangles). (b) Differential current (blue curve) overlapped to the current signal (black curve) reported in panel (a). In both panels, the current is normalized to the value of the initial unperturbed state of the first exposure. (c) Values of the maxima of the differential current from plot (b) reported as function of NO_2 concentrations with the fitting curve (red line).

which involves significant differences compared to the text chamber. Firstly, the real environment could not present a constant flow of the analyte, such as the one set in the test chamber. However, setting a variable flow is a hardly reproducible condition in laboratory and deserves diverse analysis. Secondly, the real environment is subject to variations of temperature and RH. Further analyses are ongoing to address these effects on the developed approach. Finally, the real environment could present the simultaneous presence of different gases, including oxidizing and reducing gases. Applying the method in the real environment presents the advantage that there is no a finite volume to fill-up, such as in the case of the test chamber. As such, the complexity expressed by equation (2) can be overcome, decisively simplifying the mathematical model.

4. Conclusions

In this paper, we successfully modeled the behavior of MLG-based gas sensors showing no-steady-state and scarce

recovery. We presented a mathematical approach, based on the TDSO, for devices working in a controlled test chamber. We studied the contribution of the chamber in the sensing mechanism. The TDSO approach allowed to properly fit the experimental data. The maxima of the differential current are linearly correlated to the NO_2 concentration in the range 0.12–1.32 ppm. We definitely proved that the sensors which were hardly treatable can be properly treated and calibrated when exposed to a constant injection of analyte in a finite volume chamber.

Acknowledgments

The authors warmly acknowledge M Mastrangeli and P M Sberna (Delft University of Technology, Department of Microelectronics) for the fruitful discussion and the helpful support in revisiting the manuscript. The authors also would like to thank C Schiattarella (University of Naples 'Federico II', Department of Physics 'E Pancini') for both some gas sensing measurements and useful suggestions for the data analysis as well as the authors thank the Delft University of Technology Else Kooi Lab staff for the processing support.

Author Contributions

FR performed the experimental work and the numerical simulations, analyzed the data and wrote the manuscript. TP and FR made the calculations. SV fabricated the devices. BA assisted with the sensing tests. EM developed the analytical model. PMS supervised the manuscript. All authors provided their own contribution in writing the manuscript.

ORCID iDs

Filiberto Ricciardella https://orcid.org/0000-0002-9669-5649
Sten Vollebregt https://orcid.org/0000-0001-60126180

References

[1] Neri G 2015 *Chemosensors* **3** 1
[2] Haugen J E, Tomic O and Kvaal K 2000 *Anal. Chim. Acta* **407** 23
[3] Yuan W and Shi G 2013 *J. Mater. Chem.* A **1** 10078
[4] Basu S and Bhattacharyya P 2012 *Sensors Actuators* B **173** 1
[5] Schedin F, Geim A K, Morozov S V, Hill E W, Blake P, Katsnelson M I and Novoselov K S 2007 *Nat. Mater.* **6** 652
[6] Varghese S S, Lonkar S, Singh K K, Swaminathan S and Abdala A 2015 *Sensors Actuators* B **218** 160
[7] Ratinac K R, Yang W, Ringer S P and Braet F 2010 *Environ. Sci. Technol.* **44** 1167
[8] Yavari F and Koratkar N 2012 *J. Phys. Chem. Lett.* **3** 1746
[9] Randeniya L K, Shi H, Barnard A S, Fang J, Martin P J and Ostrikov K K 2013 *Small* **9** 3993
[10] Melios C, Panchal V, Edmonds K, Lartsev A, Yakimova R and Kazakova O 2018 *ACS Sensors* **3** 1666–74
[11] Charlier J-C *et al Nanotechnology* 2009 **20** 375501
[12] Llobet E 2013 *Sensors Actuators* B **179** 32
[13] Yuan W, Liu A, Huang L, Li C and Shi G 2013 *Adv. Mater.* **25** 766
[14] Fedi F, Ricciardella F, Miglietta M L, Polichetti T, Massera E and Di Francia, G 2014 *J. Sens. Sens. Syst.* **3** 241
[15] Ricciardella F, Massera E, Polichetti T, Miglietta M L and Di Francia G 2014 *Appl. Phys. Lett.* **104** 183502
[16] Ricciardella F, Vollebregt S, Polichetti T, Alfano B, Massera E and Sarro P M 2017 *Proc. IEEE Sensors* pp 1–3
[17] Vollebregt S, Alfano B, Ricciardella F, Giesbers A J M, Grachova Y, Van Zeijl H W, Polichetti T and Sarro P M 2016 *2016 IEEE SENSORS* pp 1–3
[18] Ricciardella F, Vollebregt S, Polichetti T, Miscuglio M, Alfano B, Miglietta M L, Massera E, Di Francia G and Sarro P M 2017 *Nanoscale* **9** 6085
[19] Pearce R, Iakimov T, Andersson M, Hultman L, Spetz A L and Yakimova R 2011 *Sensors Actuators* B **155** 451
[20] Yang S, Jiang C and Wei S H 2017 *Appl. Phys. Rev.* **4** 021304
[21] Calvi A, Ferrari A, Sbuelz L, Goldoni A and Modesti S 2016 *Sensors* **16** 731
[22] Truhlar D G and Garrett B C 1980 *Acc. Chem. Res.* **13** 440
[23] Chen R J, Franklin N R, Kong J, Cao J, Tombler T W, Zhang Y and Dai H 2001 *Appl. Phys. Lett.* **79** 2258
[24] Chen G, Paronyan T M and Harutyunyan A R 2012 *Appl. Phys. Lett.* **101** 053119
[25] Dua V, Surwade S P, Ammu S, Agnihotra S R, Jain S, Roberts K E, Park S, Ruoff R S and Manohar S K 2010 *Angew. Chem. Int. Ed.* **49** 2154
[26] Wu E, Xie Y, Yuan B, Zhang H, Hu X, Liu J and Zhang D 2018 *ACS Sensors* **3** 1719–26
[27] Nomani M W K, Shishir R, Qazi M, Diwan D, Shields V B, Spencer M G, Tompa G S, Sbrockey N M and Koley G 2010 *Sensors Actuators* B **150** 301
[28] Iezhokin I, Offermans P, Brongersma S H, Giesbers A J M and Flipse C F J 2013 *Appl. Phys. Lett.* **103** 053514
[29] Hyman M P and Medlin J W 2005 *J. Phys. Chem.* B **109** 6304–10
[30] Leghrib R and Llobet E 2011 *Anal. Chim. Acta* **708** 19
[31] Behzadi Pour G and Fekri Aval L 2017 *Nano* **12** 1750096
[32] Behzadi Pour G and Fekri Aval L 2017 *Micro Nano Lett.* **13** 149
[33] Ricciardella F, Vollebregt S, Polichetti T, Alfano B, Massera E and Sarro P M 2017 *2017 IEEE Sensors* pp 1–3
[34] Leghrib R, Pavelko R, Felten A, Vasiliev A, Cané C, Gràcia I, Pireaux J J and Llobet E 2010 *Sensors Actuators* B **145** 411
[35] Ko G, Kim H-Y, Ahn J, Park Y-M, Lee K-Y and Kim J 2010 *Curr. Appl Phys.* **10** 1002
[36] Zhang Y H, Bin Chen Y, Zhou K G, Liu C H, Zeng J, Zhang H L and Peng Y 2009 *Nanotechnology* **20** 185504
[37] Leenaerts O, Partoens B and Peeters F M 2008 *Phys. Rev.* B **77** 1
[38] Behzadi Pour G, Fekri Aval L and Eslami S 2017 *Nano* **14** 1750096
[39] Behzadi Pour G and Fekri Aval L 2017 *Results Phys.* **7** 1993
[40] Behzadi Pour G 2017 *J. Nanoelectron. Optoelectron.* **12** 130
[41] Gautam M and Jayatissa A H 2011 *Mater. Sci. Eng.* C **31** 1405
[42] Mackin C, Schroeder V, Zurutuza A, Su C, Kong J, Swager T M and Palacios T 2018 *ACS Appl. Mater. Interfaces* **10** 16169–76
[43] Cervi A 2008 Caratterizzazione elettrica e spettroscopica ad impedenza di ossidi metallici nanostrutturati per il rilevamento di alcani volatili *PhD thesis* Università degli Studi di Ferrara